https://doi.org/10.5194/egusphere-2026-2987
Preprint. Discussion started: 8 July 2026

Triggering volcanic eruptions by gas bubbles accumulations in the magma chamber

Cataldo Godano[1], Massimiliano Semeraro[2], Giuseppe Gonnella[2], Giovanni Macedonio[3], Francesco Oliveri[4], Patrizia Rogolino[4], and Alessandro Sarracino[5]

[1]Dipartimento di Matematica e Fisica, Università della Campania, Viale Lincoln 5, Caserta, I-81100, Italy
[2]Dipartimento Interateneo di Fisica, Università degli Studi di Bari and INFN, Sezione di Bari, via Amendola 173, Bari I-70126, Italy
[3]Istituto Nazionale di Geofisica e Vulcanologia, Osservatorio Vesuviano, Via Diocleziano 328, Napoli I-80124, Italy
[4]Dipartimento di Scienze Matematiche e Informatiche, Scienze Fisiche e Scienze della Terra, Università di Messina, Viale Ferdinando Stagno d'Alcontres 31, Messina I-98166, Italy
[5]Dipartimento di Ingegneria, Università della Campania, Via Roma 29, Aversa I-81031, Italy

Correspondence: Cataldo Godano (cataldo.godano@unicampania.it)

Abstract. We present a model for volcanic eruptions in open-conduit condition based on the transport of batches of magma driven by the accumulation of bubbles. The viscosity of the surrounding magma counteracts gravity; however, the primary upward force acting on these bodies is driven by gas vesicles which accumulate beneath the denser bodies. Few simple and realistic assumptions lead to our theoretical model, based on the Brownian motion of colder and denser bodies embedded in a less dense and hotter magma, that can fit very well the erupted volumes distribution obtained from on field observations. Further validation is provided by extensive simulations which include all the main theoretical ingredients and, at the same time, provide additional insights on the functioning of volcanoes. Overall, the model provides a good representation of the Strombolian eruptive style. In fact, it was developed to address the apparent paradox of observing denser erupted materials embedded within a less dense magmatic medium. Furthermore, the model successfully reproduces the eruption volume distributions across various eruptive styles, suggesting that a mechanism such as coalescence underpins a more generalized framework for volcanic activity.

1 Introduction

Volcanic eruptions are complex natural geological processes depending on many characteristics of the magma composition and dynamics, thus not yet fully understood. One aspect that however is largely accepted is that one of the dominant factors controlling volcanic eruptions is the gas dissolved in the magma (Turcotte and Schubert, 2012). Indeed, together with the volcano's degassing capability, the quantity of gas in the magma, controls the explosiveness of the eruptions (Cassidy et al., 2018). This is particularly true for silicic magmas exhibiting a very high explosiveness (Jaupart and Allègre, 1991; Degruyter et al., 2012). However, explosive eruptions are also observed for basaltic magmas (Aramaki et al., 1986; Williams, 1983; Walker et al., 1984; La Spina et al., 2022) and are generally classified as Hawaiian or Strombolian (Walker, 1973; Parfitt, 2004).

https://doi.org/10.5194/egusphere-2026-2987
Preprint. Discussion started: 8 July 2026

The Hawaiian eruptions are characterized by continuous flux, generating lava fountains. These eject in the air magma bodies with a diameter ranging from some millimeters to one meter at a speed of $\simeq$100 ms^{-1}. Generally, their fallout generates sufficiently fluid lava flux (Wilson and Head III, 1981; Head III and Wilson, 1989; Tilling et al., 2010). The Strombolian eruptions are instead named after the Stromboli volcano in the Aeolian Islands in southern Italy and are characterized by a higher explosiveness (Walker, 1973; Cas and Wright, 2012). These are caused by the accumulation of gases beneath the cooler magma inside the conduit triggering an explosion (Wilson, 1980).

Many models have been developed for explaining basaltic explosive eruptions and can be divided into two different classes. The first class views the gases as trapped within the magma, where their ascent velocity dictates the resulting eruptive styles (Head III and Wilson, 1987; Parfitt and Wilson, 1994; Parfitt et al., 1995; Scandone et al., 2007). The second class, conversely, considers the gas and liquid phases to be segregated (Vergniolle and Jaupart, 1986; Jaupart and Vergniolle, 1989; Vergniolle and Brandeis, 1996; Oppenheimer et al., 2020). In this latter scenario, an unstable foam layer forms at the top of the magma chamber, generating Hawaiian eruptions when gas bubbles fail to coalesce. Conversely, Strombolian eruptions occur when bubbles coalesce into gas slugs, leading to characteristic discrete explosions (Jaupart and Vergniolle, 1988, 1989; Allard, 2010).

From a detailed statistical analysis of available data, a very interesting result has been obtained in (Papale et al., 2021), where it is shown that the erupted magma volumes are distributed according to Gamma distribution with an exponent of the power law regime equal to $-3/2$. However, such an analysis remains at a purely empirical level and a microscopic model accounting for the observed scaling has not been introduced.

In this paper, we propose a novel approach to modeling explosive volcanic eruptions. Our ultimate aim is to show that the proposed model, which is based on few simple but reasonable assumptions, can produce realistic outputs. The model we present is based on the existence of denser magma bodies within magma chambers (see discussion in Sec. 2). By allowing these bodies to diffuse and coalesce, we obtain a theoretical estimate of the probability density of erupted volumes that closely matches the experimental one. In addition, while the model was at the first instance developed for Strombolian eruptions, the result seems to be applicable to a broader range of eruptive styles. We thus speculate that our model may represent a first step towards a more general coarse-grained continuum framework capable of describing all explosive styles - from effusive to explosive and intermediate cases - by fine tuning the parameters related to gas bubbles and vesiculation. Our theoretical findings are confirmed by extensive simulations of a Brownian diffusing model which encompasses all the main ingredients of the theoretical model.

The remainder of the present paper is organized in the following way. In Sect. 2, we briefly review the existing literature about the presence of bodies of different densities in a magma chamber, in Sect. 3, we present our model and provide a theoretical prediction for the distribution of the erupted volumes reported in the volcanic eruption catalogs. In Sect. 4, we detail our numerical approach, and present a series of results confirming the theoretical prediction while also exemplifying the role of critical model parameters. And finally, in Sect. 5, we draw the conclusions of our investigation.

https://doi.org/10.5194/egusphere-2026-2987
Preprint. Discussion started: 8 July 2026

2 How denser bodies do exist

2.1 Mush formation

The presence of denser magma bodies has been discussed in the literature, especially concerning the so-called mushy zones (Cashman et al., 2017; Parmigiani et al., 2016). These are partially crystallized regions within a magma chamber where solid crystals (dendrites or grains) are surrounded by residual liquid melt (Marsh, 2006); similar structures have also been observed in molten metals during their cooling process (Barrick et al., 2017). Erupted materials with the characteristics of mushy zones have been observed, among others, at Soufrière Hills (Sparks and Young, 2002), Sakurajima (Gabellini et al., 2022) and Chaitén (Castro and Dingwell, 2009).

Here we hypothesize that, even if a large amount of literature suggests the existence of mushes on the boundaries of the magma chamber (see, among the others, Cashman et al. (2017); Caricchi et al. (2021); Humphreys et al. (2025)), some portions of the mushy zones can be moved inside the chamber due to (as example):

- convective motion triggered by density gradients associated to temperature, dissolved gases and crystals concentration inhomogeneities;
- stress caused by the gravity;
- internal stress due to the presence of fractures in the mushy zone.

A further hypothesis is that crystallization occurs at an intermediate stage and the mushy zones are not yet a dominant part of the magma chamber. As a consequence they are more free to detach from the edges of the chamber and to wander around.

2.2 The role of the dissolved gases

2.2.1 Bubble formation

For the sake of completeness, we briefly describe the mechanism of bubble formation. However, for the purposes of our model, it is sufficient to assume their existence without specifying a particular formation mechanism. We remark that vesiculation is governed by the variation of free energy (Proussevitch and Sahagian, 1996):

$$\Delta G(r) = 4\pi r^2 \gamma - \frac{4}{3}\pi r^3 \Delta P, \tag{1}$$

where γ is the surface tension magma-gas, r is the bubble radius and $\Delta P = P_g - P_m$ with P_g the gas pressure and P_m the melt pressure. When ΔG reaches its maximum at

$$r_c = \frac{2\gamma}{\Delta P}, \tag{2}$$

the bubble forms. This implies that if $r < r_c$ the bubble collapse, conversely we observe a spontaneous grow of the bubble for $r > r_c$. Substituting (2) into (1) we get the free energy variation necessary for the bubble formation

https://doi.org/10.5194/egusphere-2026-2987
Preprint. Discussion started: 8 July 2026

$$\Delta G_c = \frac{16\pi\gamma^3}{3\Delta P^2} \tag{3}$$

Notice that the inverse dependence on ΔP^2 makes easy the bubble formation even for small ΔP.

The above process is referred to as homogeneous nucleation. However, in real magma chambers a more efficient mechanism named heterogeneous nucleation occurs due to the presence of impurities which act as nucleation nuclei, increasing the rate of bubbles formation (Sparks, 1978; Hurwitz and Navon, 1994; Mangan and Sisson, 2000).

Once formed the bubble starts to move pushed by the buoyancy force (Turcotte and Schubert, 2012):

$$F_b = \frac{4}{3}\pi r^3(\rho_m - \rho_g)g \tag{4}$$

where ρ_m is the magma density and ρ_g is the one of the gas.

2.2.2 How bubbles drive mushy zones to an eruption.

The apparent paradox of the eruption of the denser materials can be explained by invoking the role of the gas bubble accumulation beneath the denser blob of magma and driving it towards the top of the magma chamber. This process, explaining the observations for the erupted mushy zones, can be generalized to the eruption of any denser magma bodies.

During its journey through the magma, the bubble can meet our denser magma batches and remains trapped because the resistance force (Tran et al., 2015):

$$F_r = \tau_y A = C\tau_y \pi r^2, \tag{5}$$

where τ_y is the yield stress and C a geometric factor taking into account the contact between the bubble and the magma batch. This means that the condition for trapping the bubble is that $F_b \leq F_r$, namely:

$$\frac{4}{3}\pi r^3(\rho_m - \rho_g)g \leq C\tau_y \pi r^2. \tag{6}$$

This gives a minimum radius for trapped bubbles

$$r_{min} = \frac{3C\tau_y}{4(\rho_m - \rho_g)g}. \tag{7}$$

A further scenario warrants discussion: a gas bubble could bypass the denser body and proceeds upwards without generating any eruption. Conversely, condition (6) can be satisfied when the viscous friction, $\tau = \mu\frac{du_z}{dx}$ (μ being the viscosity and u_z the ascent velocity of the bubble in the vertical direction), exceeds the buoyancy force instead of the yield strength τ_y. As a consequence, the viscous friction produces the same physical effect - namely, the bubble is trapped beneath the denser body, and the blob of magma can be driven into the magma conduit, thereby generating an eruption.

The trapped bubble starts to push up the batch of magma because of the buoyancy force. As a consequence, the diffusion of the denser bodies in the surrounding magma lowers the pressure in the wake of the motion (Plesset and Prosperetti, 1977; Landau and Lifshitz, 2018) and new bubbles are generated due to Eq. (3) causing the increase of the force pushing up the magma batch. In this sense our model has some similitude with the usual ones based on the gas dissolved in the magma as a triggering mechanism for the eruptions (see, as an example, Shinohara (2008) and references therein).

https://doi.org/10.5194/egusphere-2026-2987
Preprint. Discussion started: 8 July 2026

3 The model

In Fig. 1, we report a sketch of the model we develop here. The first fundamental ingredient is the existence of cold, dense and viscous magma bodies embedded in a hotter, fluid and less dense magma (see Fig. 1, left panel) as discussed in the previous section. In the following, we refer to these bodies as blobs.

Within this overall scenario, it is reasonable to hypothesize that the friction, generated by the viscosity, can contrast the sedimentation of the blobs due to gravity. This implies that the Archimedes number is ≈ 1 (Bird, 2002) and the blobs can float in the less dense magma. As a consequence, the motion of the magma bodies is mainly controlled by local convective currents due to local temperature gradients within the hotter and fluid surrounding magma. We can model this motion as a diffusion process. In addition, when two blobs come into contact, they coalesce (see Fig. 1, left panel). Admittedly, large-scale convective motion can occur within magma chambers (Turcotte and Schubert, 2012; Brandeis and Marsh, 1989; Campbell, 1996); however, this does not preclude the diffusive behavior of the blobs.

Based on the concept of sphere of influence as in (Smoluchowski, 1916; Chandrasekhar, 1943) and on dimensional arguments as discussed in Hunt (1982), it has been shown that the volume of diffusing and coalescing Brownian particles distributes according to $\sim V^{-3/2}$. Assumptions here are: i) the fluid diffusivity is inversely depending on the particles radii R; ii) particles coalesce when they come into contact. As a consequence, if we assume that our magma blobs can be approximated by spheres and that their diffusivity $D \propto 1/R$, we can explain the behavior observed by Papale et al. (2021), at least for the power law regime of the erupted material, getting for the volume distribution

$$p(V) \sim V^{-\frac{3}{2}} \ . \tag{8}$$

The second ingredient of the model is gas vesiculation beneath blobs, which generates a force pushing them upwards. As gas bubbles keep accumulating beneath the blobs during their motion, this force increases with time and the blob is transported towards the conduit until an eruption event occurs (see Fig. 1, right panel).

For simplicity, we assume that the force pushing the blobs upwards increases linearly in time with constant rate λ. The specific value of λ takes into account all factors affecting how fast vesiculation occurs, gas bubbles migrate inside the viscous magma, magma compositions or blob geometries. An eruption thus occurs as soon as the buoyancy force provided by the vesiculation equals the gravity force acting on the blob, which is the base-line condition for which the blob rises. In symbols, we have

$$\lambda \Delta t = \rho g V_e \ , \tag{9}$$

where λ is the increasing rate of the buoyancy force generated by the vesiculation, Δt is the time interval between two successive eruptions, ρ is the density of the blob and V_e is the volume of the incoming eruption.

In what follows, we assume a Poissonian model for the temporal occurrence De la Cruz-Reyna (1991); Bottiglieri et al. (2005); Papale (2018). As a consequence, Δt follows an exponential distribution:

$$p_{\Delta t}(\Delta t) = \mu e^{-\mu \Delta t} \ , \tag{10}$$

https://doi.org/10.5194/egusphere-2026-2987
Preprint. Discussion started: 8 July 2026

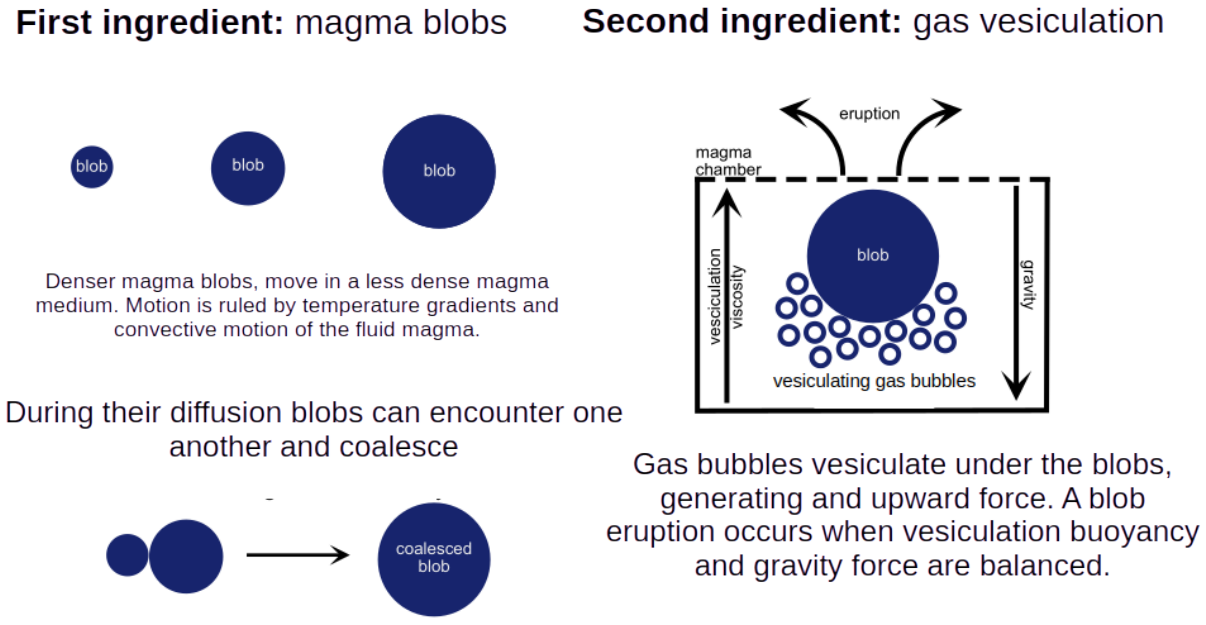

Figure 1. Schematic illustration of the model. The left panel depicts the first key ingredient, i.e. magma blobs and their ability to coalesce. The right panel shows the second ingredient, i.e. gas vesiculation, within a richer representation that includes the magma chamber, directions of all relevant forces and eruption phenomena.

where μ is the inverse of the mean time interval between two successive eruptions, and using Eq. (9) we get the distribution of the potentially erupted volumes V_e:

$$p_{V_e}(V_e) = \frac{\rho g \mu}{\lambda} e^{-\frac{\rho g \mu}{\lambda} V_e} . \tag{11}$$

Finally, the joint probability to have a blob of volume V and an eruption of volume $V_e = V$ is

$$p(V) = \frac{\beta^{\alpha+1}}{\Gamma(\alpha+1)} V^{\alpha} e^{-\beta V}, \tag{12}$$

where $\alpha = -3/2$, Γ is the gamma function and $\beta = \rho g \mu / \lambda$.

Fig. 2 shows the experimental distribution of the erupted volumes obtained from the Volcano Global Risk Identification and Analysis Project (VOGRIPA) catalog (Crosweller et al., 2012) fitted (in a χ^2 sense) by the red line representing Eq. (12) with $\beta = 5 \cdot 10^{-4}$. This implies that the exponential decay becomes dominant, with respect to the power law term, at $2 \cdot 10^3$ Mm^3.

It can be noted that the experimental $p(V)$ is not fitted for $V < 0.7$ Mm^3. This can be explained by the incompleteness of the catalog. More precisely, it is reasonable to assume that not all small eruptions ($V < 0.7$ Mm^3) are reported in the catalog as many of these are covered by larger ones occurred at later times.

https://doi.org/10.5194/egusphere-2026-2987
Preprint. Discussion started: 8 July 2026

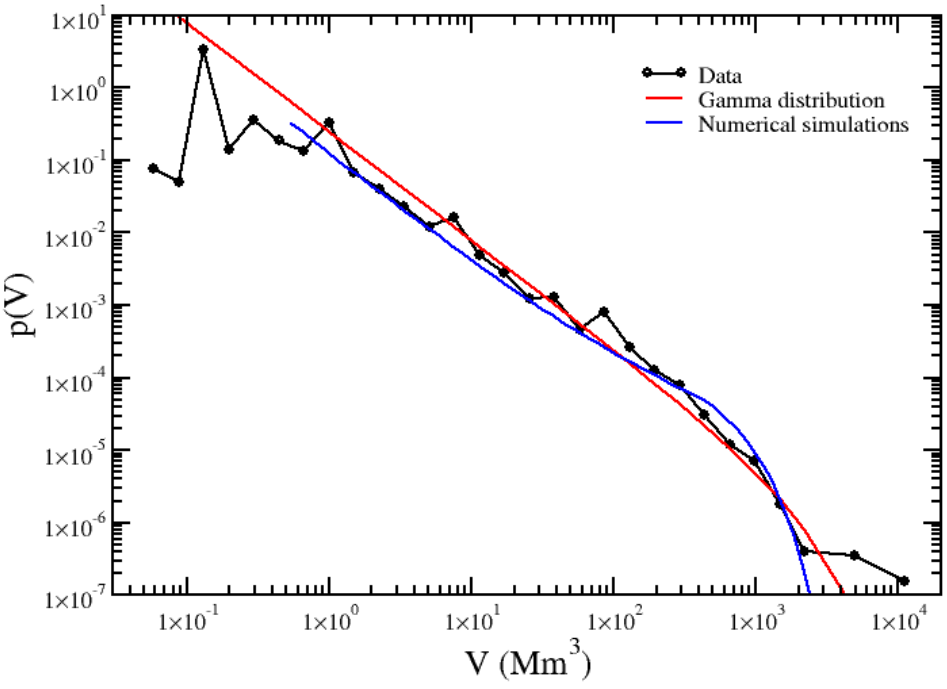

Figure 2. The experimental distribution of V (black dots). The red line represents the χ^2 fit using the parameters reported in the text. The blue line is the distribution of the erupted volumes obtained by the numerical simulations for $N = 300$ (being this one the best fitting curve in a χ^2 sense). Here we used the volume eruptions catalogue of the Volcano Global Risk Identification and Analysis Project (VOGRIPA) (Crosweller et al., 2012) limited to small eruptions. Another catalogue, including larger eruptions, is provided by the Smithsonian Institution (Venzke, 2013). However we limit ourselves to the first one in order to avoid mixing of not homogeneous catalogues.

4 Numerical Validation

In order to validate our prediction Eq. (12), we perform extensive numerical simulations adopting molecular dynamics techniques adapted from Brownian motion modeling (Carollo et al., 2023; Semeraro et al., 2023). The model we numerically explore is based on Brownian dynamics, is reminiscent of (Hunt, 1982) and includes all the ingredients of the theoretical recipe from Sect. 3. In particular, in Sect. 4.1, we detail the precise model we implemented (Godano, 2026), in Sect. 4.2, we provide details on numerical integration and mapping to physical units, and finally in Sect. 4.3, we provide a overview of numerical outputs at the same exemplifying how simulations reproduce experimental data and also providing additional insights on the model functioning.

https://doi.org/10.5194/egusphere-2026-2987
Preprint. Discussion started: 8 July 2026

4.1 Model

The setting of our model is a three-dimensional box of side L which contains a viscous magma of density ρ_m and viscosity η. In the box there are N blobs of magma with larger density $\rho_d > \rho_m$ which are modeled as diffusing spherical Brownian particles with radii $R_i(t)$, $i = 1, \dots, N$. This implements the first ingredient from Sect. 3. Note that blob radii feature a time dependency as they undergo coalescence phenomena. More specifically, when the distance between the centers of any two blobs, say the i-th and the j-th, is such that $d_{ij}(t) \leq R_i(t) + R_j(t)$, the smaller blob is absorbed by the bigger one. The latter thus acquires a new radius $R'_i(t)$ such that the total volume of the two original blobs is conserved, i.e. $R'_i(t) = (R_i^3(t) + R_j^3(t))^{1/3}$, whereas the former is removed. At the same time a new blob is positioned at a random location in the box, so that the total number of blobs N is conserved. We remark that this approach enables us to simultaneously account for magma blobs from the volcanological framework and particle coalescence results (Smoluchowski, 1916; Chandrasekhar, 1943; Hunt, 1982) within a simplified setting that does not rely on detailed magma chamber specifications. The results presented in the following refer to the case in which all of new blobs are given an initial radius extracted from a power-law distribution $p(R) \sim R^{-5/2}$ ranged in the small closed interval $[0.1, 1.0]$. This is a choice of convenience, as this corresponds to introducing new blobs with volumes distributed according to $p(V) \sim V^{-3/2}$, thus helping to rapidly reach and maintain the stationary configuration prescribed by (Smoluchowski, 1916; Chandrasekhar, 1943; Hunt, 1982). However, we checked that, apart from small deviations, similar results concerning the distribution for the erupted volumes are obtained considering new radii with fixed unitary length, or extracted from a constant distribution, or even from a power-law one with exponent slightly different from $-5/2$.

The dynamics of the i-th blob in the box is ruled by the following Langevin equation

$$m_i(t)\dot{\boldsymbol{v}}_i(t) = -\gamma_i(t)\boldsymbol{v}_i(t) + \boldsymbol{F}_{g,i}(t) + \boldsymbol{F}_{up,i}(t) + \sqrt{2\gamma_i(t)k_BT}\,\boldsymbol{\xi}_i(t)\,, \tag{13}$$

where $m_i(t) = V_i(t)\rho_d = 4\pi R_i^3(t)\rho_d/3$ is the mass of the blob, $\boldsymbol{v}_i(t)$ is its velocity, $\gamma_i(t) = 6\pi\eta R_i(t)$ is the Stokes viscous coefficient, which explicitly depends on the time-dependent radius, k_B is the Boltzmann constant, T is the system temperature,

$$\boldsymbol{F}_{g,i}(t) = -V_i(t)\Delta\rho_{dm}g\hat{k} = -\frac{4}{3}\pi R_i^3(t)\Delta\rho_{dm}g\hat{k} \tag{14}$$

is the gravity force pushing blobs downwards ($\hat{k}$ z-direction versor), and $\boldsymbol{\xi}_i(t)$ is a Gaussian white noise satisfying $\langle\xi_{i,l}(t)\rangle = 0$ and $\langle\xi_{i,l}(t)\xi_{j,m}(t')\rangle = \delta_{ij}\delta_{lm}\delta(t-t')$ ($l, m = x, y, z$, dimensional indices). The further term

$$\boldsymbol{F}_{up,i}(t) = V_{v,i}(t)\Delta\rho_{vm}g\hat{k} \tag{15}$$

represents a force pushing blobs upwards due to the action of vesicles of density ρ_v accumulating beneath each blob ($\Delta\rho_{vm} = \rho_v - \rho_m$), with $V_{v,i}(t)$ total volume of the vesicles under the i-th blob increasing over time. This implements the second ingredient from Sec. 3. For simplicity, we assume a linear time trend $V_{v,i}(t) = \alpha(t - \tau_{V,i})$, where $\tau_{V,i}$ denotes the birthing time of the i-th blob. For blobs which have not yet coalesced, this is 0. For coalescing blobs, the larger one driving the merging phenomenon inherits the $\tau_{V,i}$ of the larger colliding blob, while the smaller one is associated a $\tau_{V,i}$ extracted from the exponential distribution $p(\tau_{V,i}) = e^{-\tau_{V,i}/\tau_s}/\tau_s$, $\tau_s > 0$.

https://doi.org/10.5194/egusphere-2026-2987
Preprint. Discussion started: 8 July 2026

Due to the large magma viscosity, inertial effects in Eq. (13) can be neglected, thus obtaining the following overdamped Langevin equation

$$\gamma_i(t)\dot{\mathbf{r}}_i(t) = \boldsymbol{F}_{g,i}(t) + \boldsymbol{F}_{up,i}(t) + \sqrt{2\gamma_i(t)k_BT}\boldsymbol{\xi}_i(t) \,, \tag{16}$$

with $\boldsymbol{r}_i(t)$ location of the i-th blob inside the box and $\dot{\boldsymbol{r}}_i(t) \equiv \boldsymbol{v}_i(t)$. Note that all viscous coefficients are positive, i.e. $\gamma_i(t) = 6\pi\eta R_i(t) > 0$, thus Eq. (16) can be recast in the following form

$$\dot{r}_i(t) = \boldsymbol{f}_{g,i}(t) + \boldsymbol{f}_{up,i}(t) + \sqrt{2\frac{k_BT}{\gamma_i(t)}}\,\boldsymbol{\xi}_i(t) \,, \tag{17}$$

where

$$\boldsymbol{f}_{g,i}(t) = \frac{\boldsymbol{F}_{g,i}(t)}{\gamma_i(t)} = -\frac{2}{9}\frac{R_i^2(t)}{\eta}\Delta\rho_{dm}g\hat{k} \,, \tag{18}$$

and

$$\boldsymbol{f}_{up,i}(t) = \frac{\boldsymbol{F}_{up,i}(t)}{\gamma_i(t)} = \frac{V_{v,i}(t)}{6\pi\eta R_i(t)}\Delta\rho_{vm}g\hat{k} \,. \tag{19}$$

Note that the term $k_BT/\gamma_i(t)$ in Eq. (17) represents the diffusion coefficient for a single blob without gravity and upwards forces. The diffusion coefficient thus naturally depends on the inverse of the blob radius, as assumed in Sect. 3. In the following we actually assume that the viscosity of the magma in the box is very large, so that the gravity force can be neglected. The Langevin equations we numerically integrate thus become

$$_i(t) = \boldsymbol{f}_{up,i}(t) + \sqrt{2\frac{k_BT}{\gamma_i(t)}}\,\boldsymbol{\xi}_i(t) \,. \tag{20}$$

The eruption mechanism is implemented in the following way. Whenever a blob, say the i-th, reaches the top face of the box, its volume is recorded and the blob is removed. At the same time, a new blob is positioned at a random location, so that the total number of blobs N is yet conserved, and is associated a radius similarly to the case of coalescence phenomena. All other faces of the box are instead interpreted as walls of the magma chamber, hence whenever the blob reaches them it simply bounces back.

4.2 Methods

We perform numerical integration of Eq. (20) through the Euler-Maruyama integrator (Kloeden and Platen, 1992). Actual implementation was performed by writing our script from scratch in C including specific subroutines for particle bouncing on the lateral and bottom box sides, blob eruption and blob coalescence, as well as for introduction of new blobs with radii extracted from different distributions. Throughout all simulation runs we set the integration timestep at $dt = 10^{-3}$ for numerical stability and fix $L = 100$, $\Delta\rho_{vm} = 1$, $\alpha = 10^{-4}$, $k_BT = 1$, $6\pi\eta = 1$ and $\tau_s = 1$. The radii of new particles introduced following coalescence and eruption events are sampled from a power-law distribution $p(R) \sim R^{-5/2}$ bounded within the range $[0.1, 1.0]$.

https://doi.org/10.5194/egusphere-2026-2987
Preprint. Discussion started: 8 July 2026

Together with $\epsilon = k_B T$ and τ_s, the arbitrary but simple length $l = L/100 = 1$ set the reduced energy, time and length units of our simulations. All other units are obtained as combinations of these. At each timestep we control wether particles bounce back at lateral and bottom sides of the box or are erupted through the top one. For all choices of N, we initially place the N particles inside the box at random locations and let the system evolve for $10\tau_s$, i.e for 10^4 dt. In such a way the system thermalizes and reaches a stationary configuration, a sample instance of which is reported in Fig. 3 for $N = 100$. Then, we let the system evolve for further $5 \cdot 10^2 \tau_s$, i.e. for $5 \cdot 10^5$ dt, and during this time interval we cumulatively sampled the erupted volumes, i.e. the volumes of the particles that reached the top of the box. In order to enhance the sampling statistics, we generated $p(V)$ distributions by combining data from 100 independent runs for each choice of N. We performed simulation in serial mode on single core, and each simulation run required 24–72 hours to complete depending on the value of N.

Mapping of reduced units into physical ones is readily obtained. Concerning length, magma chamber have dimensions of order $\sim 10^4$ m, so $l \sim 10^2$ m. Note that this translates into a factor $\sim 10^7 - 10^8$ in terms of volumes, which is exactly the order of the factor we used to rescale numerical data in Fig. 2. As for time, eruptions last for days, while blobs are emitted continuously, so it is reasonable to assume that in case of Strombolian eruptions τ_s is of the order of hours. In terms of physical units, we thus get that $\tau_s \sim 10^3$ s, and that the total simulation time amounts to $5-6$ days. However, (Sanchez and Shcherbakov, 2012) showed that the distribution of the time intervals between consecutive eruptions, or intertimes, becomes independent of the volcanic style when τ_s is normalized for the average intertime. Concerning energy, we adopted the convention to set the Boltzmann constant k_B to one. Accordingly, temperature and energy quantities have the same dimensions. As it is a know fact that lava melts at $\sim 10^3$ K, we thus get $\epsilon \sim 10^3$ K.

4.3 Output

In Fig. 4, we report the distribution of erupted volumes $p(V)$ for different values of N in reduced units. For all values of N, these share a common trait, i.e. a trend $\sim V^{-3/2}$ over three decades. We remark that all simulations are started and progress in a stationary configuration. We in fact checked that the shape of the curves shown in Fig. 4 does not change varying the sampling window. Interestingly, in Fig. 5, we show that, although a similar initial trend, the actual value of N affects the overall blob-volume-over-box-volume ratio, which increases with N but remains stationary over time for each N.

Concerning instead the right tail, we observe a cutoff volume after which distributions decrease (essentially) exponentially. We remark that as N is increased, the probability for the eruption of larger blobs becomes larger. This is in agreement with the intuitive idea that, as the total number of blobs is increased, these can coalesce more frequently, and thus result in larger blobs that can be erupted. We also note that the change of trends, from power-law to exponential, occurs for critical values of volume increasing with N. As for comparison with experimental data, a visual comparison between Fig. 2 and Fig. 4 already reveals that numerical and experimental curves are very similar. More quantitatively, in order to compare data directly, we first transformed numerical data from reduced to physical units, and then compared the resulting curves with the experimental one from Fig. 2. Here we report a comparison between the experimental curve and the numerical one for $N = 300$, with which a good agreement (and best with respect to all values of N examined) is found.

https://doi.org/10.5194/egusphere-2026-2987
Preprint. Discussion started: 8 July 2026

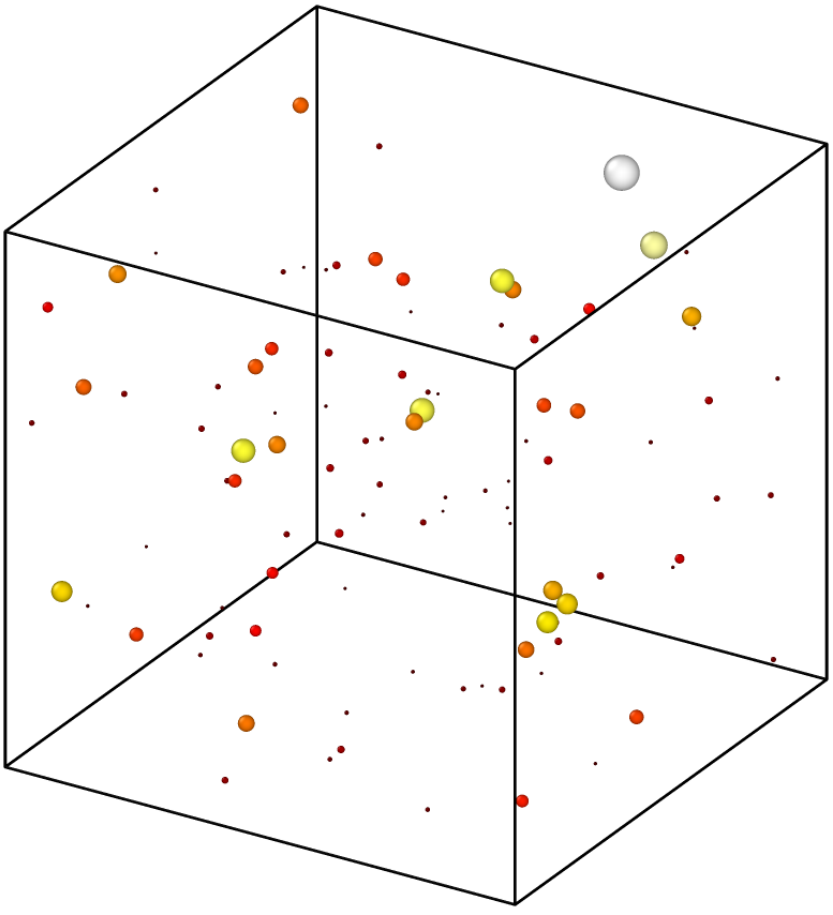

Figure 3. Sample stationary configuration of the model for $N = 100$. Black lines denote the box edges, while particles are colored from black to white through red according to their radii. Simulation parameters are detailed in Sec. 4.2.

In Fig.6, we report the distribution of the intertimes τ_{er}, i.e. the time intervals between consecutive blob eruptions, for different values of N. For all values of N, data show a clear decreasing exponential trend, as highlighted by the semi-log representation. This first remark confirms our assumption of Poissonian distribution for eruption occurrences from Sec. 3. We remark that the only exception to a monotonous trend is found for $N = 500$. As intuitively expected, when the number of
260 blobs is large enough, small particles reintroduced close to the top of the box can be erupted rapidly and, more importantly, more frequently (similar comments apply to the case of more intense upward force, see the inset of Fig. 7). Note that, as N is increased, the slope of the curves reduces, denoting a larger probability for lower τ_{er} values. This is in agreement with the

https://doi.org/10.5194/egusphere-2026-2987
Preprint. Discussion started: 8 July 2026

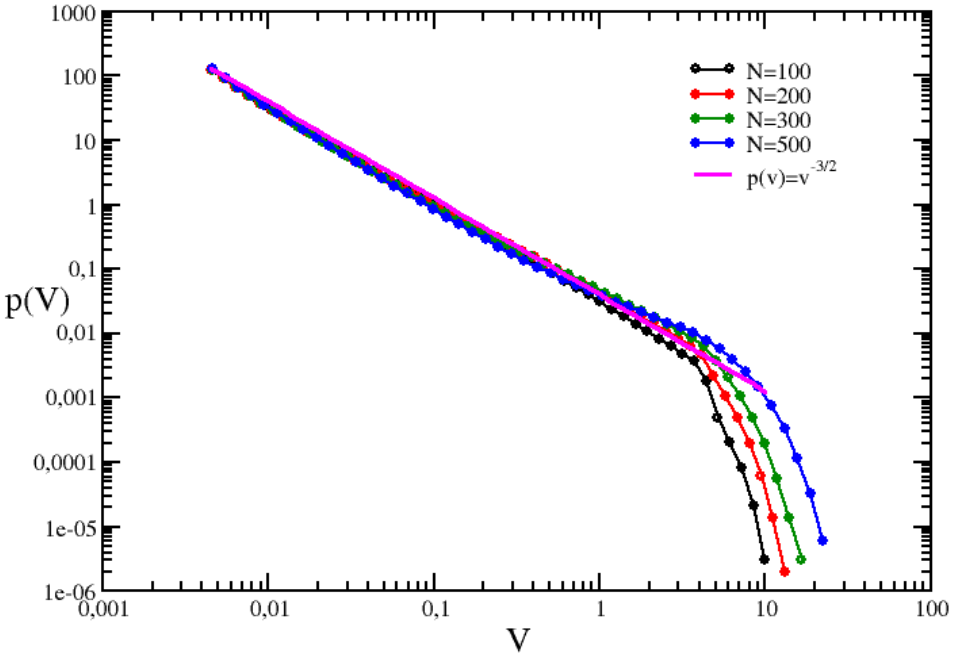

Figure 4. Distribution $p(V)$ of the volumes of the erupted blobs for different values of N. The magenta line highlights the trend $\sim V^{-3/2}$. Simulation parameters are detailed in Sec. 4.2. Simulation parameters and data here are given in reduced units.

intuitive idea that, as the total number of blobs is increased, these can coalesce more frequently, thus resulting in larger erupted volumes (see Fig. 4). More quantitatively, we performed fit of our data with the functional form $f(\tau_{er}) = n\, e^{-\tau_{er}/\tau_c}$, where n and τ_c are the fit parameters and are respectively interpreted as a normalization constant and a characteristic time for eruptions, obtaining $\tau_c \sim 3.3,\ 1.6,\ 1.1$ and 0.5 for $N = 100, 200, 300$ and 500, respectively (the resulting functional form are reported in Fig.6 as black lines). As expected, our τ_c estimates reduce as N increases. Moreover, we observe that mapping these estimates into physical units, we obtain a range of characteristic times spanning from about 3 days for $N = 100$ to about 12 hours for $N = 500$.

In Fig.7, we instead investigate how varying α in the expression for the linear upward force affects the distribution of erupted volumes once the number of blobs is fixed at $N = 100$. The figure clearly shows that for all α values we investigated, the main part of the distributions follows a $V^{-3/2}$ trend (see the magenta line) and is essentially unaffected by these changes. We thus conclude that its shape and trend are only driven by how particles are reintroduced after coalescence and eruption occurrences. As for the right tail, we instead observe a richer scenario. When α is increased to $\alpha = 10^{-3}$, the right tail decreases faster than for $\alpha = 10^{-4}$. This effect reflects the fact that in this case blobs are subjected to a more intense upward push and, as

https://doi.org/10.5194/egusphere-2026-2987
Preprint. Discussion started: 8 July 2026

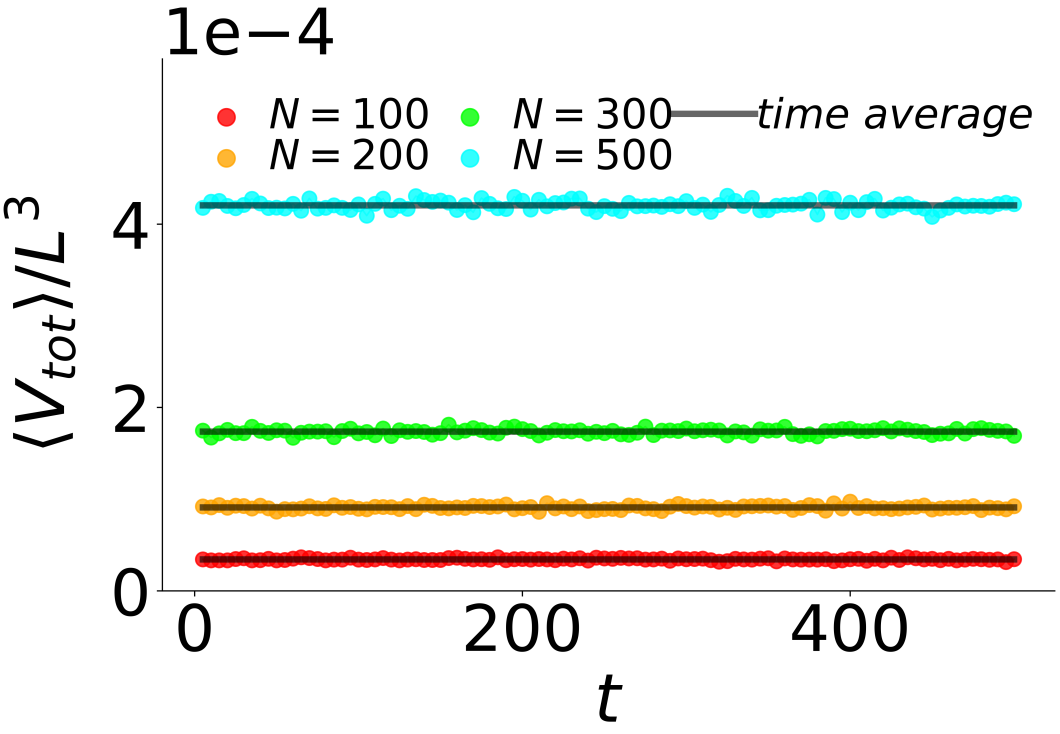

Figure 5. Time trend of the total blob volume over the total simulation box for different values of N. Black lines report time averages. Simulation parameters are detailed in Sec. 4.2. Data are averaged over 50 independent runs.

shown by the inset reporting the intertimes distributions, are erupted on average more rapidly ($\tau_c \sim 1.25$ rather than ~ 3.3). As a consequence, these have less chances to collide, coalesce and generate larger blobs, hence the lower probability for large volumes. When α is reduced to $\alpha = 10^{-5}$ the effect is instead opposite: blobs are erupted on average less frequently (see inset, $\tau_c \sim 4.7$), and thus have more chances to coalesce into larger ones, hence the higher probability for larger volumes. Interestingly, the overall shape of the distribution in this case closely resembles the ones obtained for larger N, which in turn better agrees with experimental data (see Fig. 2 and Fig. 4). We thus conclude that acting on the intensity of the upward-pushing force by tuning α or changing the number of blobs N in the system produce similar effects as in both cases one interferes with the likeliness of blobs to collide and coalesce into larger ones.

5 Conclusions

We present a model for volcanic eruptions in open-conduit condition (eg: Strombolian) based on some very simple but realistic assumptions. In the magma chamber there exist some bodies of denser magma, or blobs, embedded in a less dense and viscous magma. The viscosity contrasts the gravity of the blobs whose motion is considered diffusive and driven by temperature gradients and small local convective motion occurring in the embedding fluid. The blobs coalesce upon collision. The eruption

https://doi.org/10.5194/egusphere-2026-2987
Preprint. Discussion started: 8 July 2026

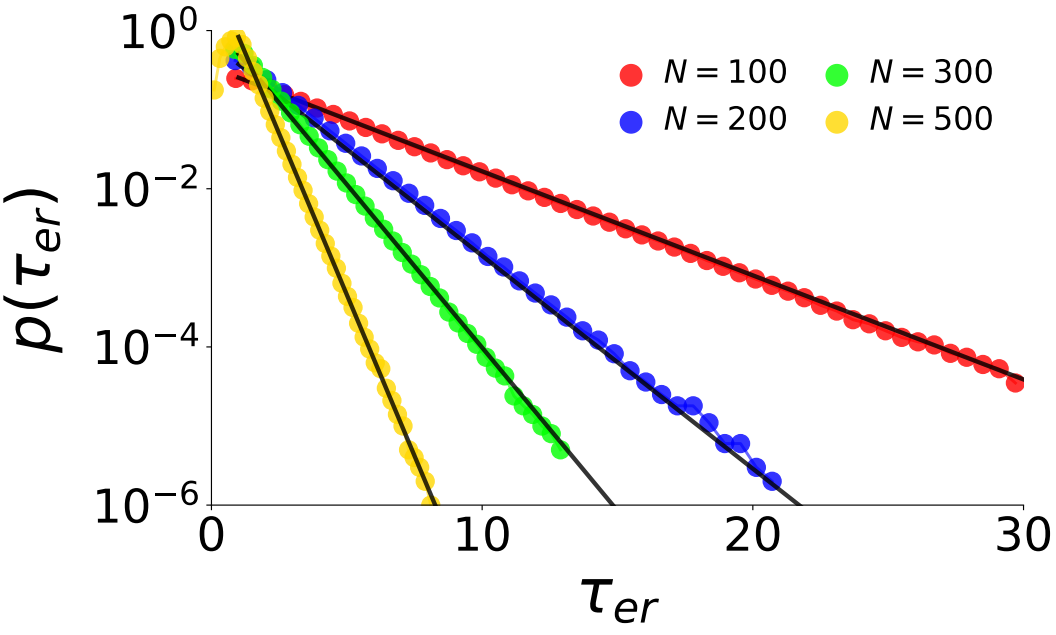

Figure 6. Distribution $p(\tau_{er})$ of the intertimes τ_r between consecutive blob eruptions for different values of N. Black lines report fit performed with the functional form $f(\tau_{er}) = n\ e^{-\tau_{er}/\tau_c}$, with n (normalization constant) and τ_c (characteristic time) fit parameters. Simulation parameters are detailed in Sec. 4.2.

are caused by the vesiculation beneath the blobs of gases dissolved in the less dense magma. When the buoyancy force provided by the vesiculated gases is larger than the combined gravity and viscous forces acting on the blobs, these are pushed upwards causing an eruption. Eruptions occurrences are assumed to follow a Poisson distribution. On the basis of these assumptions and the scaling results of Smoluchowski (1916); Chandrasekhar (1943); Hunt (1982), we derive an analytical expression for the probability distribution of the erupted volumes which agrees very well with observations. Numerical simulations based on molecular dynamics techniques and including the above assumptions, produce erupted volume distributions in good agreement with both the analytical and experimental ones, and thus validate our results. In particular, the proposed model accounts for the observed scaling behavior of the erupted volumes of magma $p(V) \sim V^{-3/2}$ reported in Papale et al. (2021), and for the exponential cutoff at large volumes.

Many aspects of volcanic eruption mechanisms, such as interactions with crust, conduit dynamics, and the supply of fresh magma from depth, are neglected in our model. However, we seek to investigate the statistical consequences of stochastic coalescence dynamics within the simplest possible framework, without attempting to incorporate the full complexity of magma transport, dyking processes, viscoelastic crustal response, or transcrustal reservoir connectivity.

We speculate that our model could actually represent the first step towards a more general coarse-grained continuum model which could account for all explosive styles at once, from effusive to explosive, by fine tuning some general features related to gas bubbles and vesiculation. This is left to possible future implementation.

https://doi.org/10.5194/egusphere-2026-2987
Preprint. Discussion started: 8 July 2026

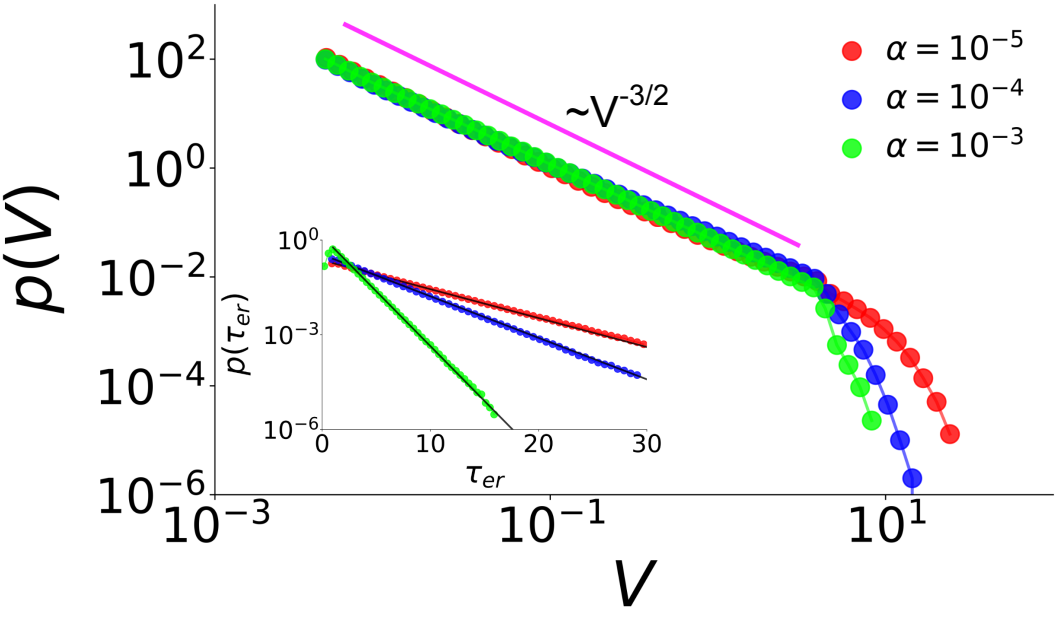

Figure 7. Distribution $p(V)$ of the volumes of the erupted blobs for different values of α in Eq.(19). The magenta line highlights the trend $\sim V^{-3/2}$. The inset reports the corresponding distribution $p(\tau_{er})$ of the intertimes τ_r between consecutive blob eruptions. Here black lines report fit performed with the functional form $f(\tau_{er}) = n\, e^{-\tau_{er}/\tau_c}$, with n (normalization constant) and τ_c (characteristic time) fit parameters. Simulation parameters are detailed in Sec. 4.2.

Code availability. The simulation code can be downloaded at https://doi.org/10.5281/zenodo.20519874

(Godano, 2026)

Data availability. The VOGRIPA catalog of volcanic eruptions is available at https://vogripa.org/searchVOGRIPA.cfc?method=searchForm.

Author contributions. All the author equally contributed to the paper.

Competing interests. The authors declare no conflict of interest. The product of the present study will be only used only for scientific purposes.

Acknowledgements. All authors (C.G., M.S. G.G., G.M., F.O., P.R. and A.S.) acknowledge the Smithsonian Institute for providing the volcano catalog. Numerical calculations have been made possible through a CINECA-INFN agreement, providing access to HPC resources

https://doi.org/10.5194/egusphere-2026-2987
Preprint. Discussion started: 8 July 2026

at CINECA. C.G., M.S., G.G., F.O. and P.R. acknowledge MUR project PRIN 2022 PNRR P20222B5P9 for partial financial support. M.S. and G.G. acknowledge support from INFN/FIELDTURB project and from MUR projects PRIN 2020/PFCXPE and Quantum Sensing and Modelling for One-Health (QuaSiModO).

https://doi.org/10.5194/egusphere-2026-2987
Preprint. Discussion started: 8 July 2026

References

Allard, P.: A Co2-rich gas trigger of explosive paroxysms at Stromboli basaltic volcano, Italy, J. Volcanol. Geoth. Res., 189, 363–374, https://www.sciencedirect.com/science/article/abs/pii/S0377027309004545, 2010.

Aramaki, S., Hayakawa, Y., Fujii, T., Nakamura, K., and Fukuoka, T.: The October 1983 eruption of Miyakejima volcano, J. Volcanol. Geotherm. Res., 29, 203–229, https://www.sciencedirect.com/science/article/abs/pii/0377027386900454, 1986.

Barrick, E. J., Jain, D., DuPont, J. N., and Seidman, D. N.: Effects of heating and cooling rates on phase transformations in 10 wt pct Ni steel and their application to gas tungsten arc welding, Metallurgical and Materials Transactions A, 48, 5890–5910, 2017.

Bird, R. B.: Transport phenomena, Appl. Mech. Rev., 55, R1–R4, https://www.wiley.com/en-us/Transport+Phenomena%2C+Revised+2nd+Edition-p-9780470115398, 2002.

Bottiglieri, M., De Martino, S., Falanga, M., Godano, C., and Palo, M.: Statistics of inter-time of Strombolian explosion-quakes, EPL (Europhysics Letters), 72, 493–498, 2005.

Brandeis, G. and Marsh, B. D.: The convective liquidus in a solidifying magma chamber: a fluid dynamic investigation, Nature, 339, 613–616, https://www.nature.com/articles/339613a0#about-the-journal, 1989.

Campbell, I. H.: Fluid dynamic processes in basaltic magma chambers, in: Develo. Petrol., vol. 15, pp. 45–76, Elsevier, https://www.sciencedirect.com/science/article/abs/pii/S0167289496800042, 1996.

Caricchi, L., Townsend, M., Rivalta, E., and Namiki, A.: The build-up and triggers of volcanic eruptions, Nat. Rev. Earth Environ., 2, 458–476, https://doi.org/10.1038/s43017-021-00174-8, 2021.

Carollo, G. B., Semeraro, M., Gonnella, G., and Zamparo, M.: Work fluctuations for a confined Brownian particle: the role of initial conditions, J. Phys. A, 56, 435 003, https://doi.org/10.1088/1751-8121/acfc09, 2023.

Cas, R. and Wright, J.: Volcanic successions modern and ancient: A geological approach to processes, products and successions, Springer Science & Business Media, https://link.springer.com/book/10.1007/978-94-009-3167-1, 2012.

Cashman, K. V., Sparks, R. S. J., and Blundy, J. D.: Vertically extensive and unstable magmatic systems: a unified view of igneous processes, Science, 355, eaag3055, 2017.

Cassidy, M., Manga, M., Cashman, K., and Bachmann, O.: Controls on explosive-effusive volcanic eruption styles, Nat. Comm., 9, 2839, https://www.nature.com/articles/s41467-018-05293-3, 2018.

Castro, J. M. and Dingwell, D. B.: Rapid ascent of rhyolitic magma at Chaitén volcano, Chile, Nature, 461, 780–783, 2009.

Chandrasekhar, S.: Stochastic problems in physics and astronomy, Rev. Mod. Phys., 15, 1, https://journals.aps.org/rmp/abstract/10.1103/RevModPhys.15.1, 1943.

Crosweller, H. S., Arora, B., Brown, S. K., Cottrell, E., Deligne, N. I., Guerrero, N. O., Hobbs, L., Kiyosugi, K., Loughlin, S. C., Lowndes, J., Nayembil, M., Siebert, L., Sparks, R. S. J., Takarada, S., and Venzke, E.: Global database on large magnitude explosive volcanic eruptions (LaMEVE), J. Appl. Volcanol., 1, 1–13, https://appliedvolc.biomedcentral.com/articles/10.1186/2191-5040-1-4, 2012.

De la Cruz-Reyna, S.: Poisson-distributed patterns of explosive eruptive activity, Bulletin of Volcanology, 54, 57–67, 1991.

Degruyter, W., Bachmann, O., Burgisser, A., and Manga, M.: The effects of outgassing on the transition between effusive and explosive silicic eruptions, Earth Planet. Sci. Lett., 349, 161–170, https://www.sciencedirect.com/science/article/abs/pii/S0012821X12003482, 2012.

Gabellini, P., Cioni, R., Geshi, N., Pistolesi, M., Miwa, T., Lacanna, G., and Ripepe, M.: Eruptive dynamics and fragmentation mechanisms during cyclic Vulcanian activity at Sakurajima volcano (Japan): Insights from ash texture analysis, Journal of Volcanology and Geothermal Research, 428, 107 582, 2022.

https://doi.org/10.5194/egusphere-2026-2987
Preprint. Discussion started: 8 July 2026

Godano, C.: Simulation code, https://doi.org/10.5281/zenodo.20355974, 2026.

Head III, J. W. and Wilson, L.: Lava fountain heights at Pu'u'O'o, Kilauea, Hawaii: Indicators of amount and variations of exsolved magma volatiles, J. Geophys. Res., 92, 13 715–13 719, https://agupubs.onlinelibrary.wiley.com/doi/abs/10.1029/JB092IB13P13715, 1987.

Head III, J. W. and Wilson, L.: Basaltic pyroclastic eruptions: influence of gas-release patterns and volume fluxes on fountain structure, and the formation of cinder cones, spatter cones, rootless flows, lava ponds and lava flows, J. Volcanol. Geoth. Res., 37, 261–271, https://www.sciencedirect.com/science/article/abs/pii/0377027389900838, 1989.

Humphreys, M. C. S., Namur, O., Bohrson, W. A., Bouilhol, P., Cooper, G. F., Cooper, K. M., Huber, C., Lissenberg, C. J., Morgado, E., and Spera, F. J.: Crystal mush processes and crustal magmatism, Nat. Rev. Earth Environ., 6, 401–416, https://doi.org/10.1038/s43017-025-00682-x, 2025.

Hunt, J. R.: Self-similar particle-size distributions during coagulation: theory and experimental verification, J. Fluid Mech., 122, 169–185, https://doi.org/10.1017/S0022112082002158, 1982.

Hurwitz, S. and Navon, O.: Bubble nucleation in rhyolitic melts: Experiments at high pressure, temperature, and water content, Earth Planet. Sci. Lett., 122, 267–280, https://doi.org/10.1016/0012-821X(94)90001-9, 1994.

Jaupart, C. and Allègre, C. J.: Gas content, eruption rate and instabilities of eruption regime in silicic volcanoes, Earth Planet. Sci. Lett., 102, 413–429, https://www.sciencedirect.com/science/article/abs/pii/0012821X9190032D, 1991.

Jaupart, C. and Vergniolle, S.: Laboratory models of Hawaiian and Strombolian eruptions, Nature, 331, 58–60, https://www.nature.com/articles/331058a0, 1988.

Jaupart, C. and Vergniolle, S.: The generation and collapse of a foam layer at the roof of a basaltic magma chamber, J. Fluid Mech., 203, 347–380, https://doi.org/10.1017/S0022112089001497, 1989.

Kloeden, P. E. and Platen, E.: Numerical Solution of Stochastic Differential Equations, Springer, https://link.springer.com/book/10.1007/978-3-662-12616-5, 1992.

La Spina, G., Arzilli, F., Burton, M. R., Polacci, M., and Clarke, A. B.: Role of volatiles in highly explosive basaltic eruptions, Comm. Earth Environ., 3, 156, https://www.nature.com/articles/s43247-022-00479-6, 2022.

Landau, L. D. and Lifshitz, E. M.: Fluid Mechanics - Second Edition, Oxford University Press, Oxford, https://www.cambridge.org/it/universitypress/subjects/physics/nonlinear-science-and-fluid-dynamics/fluid-mechanics-2nd-edition?format=HB, 2018.

Mangan, M. and Sisson, T.: Delayed, disequilibrium degassing in rhyolite magma: decompression experiments and implications for explosive volcanism, Earth Planet. Sci. Lett., 183, 441–455, https://doi.org/10.1016/S0012-821X(00)00299-5, 2000.

Marsh, B. D.: Dynamics of magmatic systems, Elements, 2, 287–292, 2006.

Oppenheimer, J., Capponi, A., Cashman, K. V., Lane, S. J., Rust, A. C., and James, M. R.: Analogue experiments on the rise of large bubbles through a solids-rich suspension: A "weak plug" model for Strombolian eruptions, Earth Planet. Sci. Lett., 531, 115 931, https://www.sciencedirect.com/science/article/abs/pii/S0012821X19306235, 2020.

Papale, P.: Global time-size distribution of volcanic eruptions on Earth, Scientific reports, 8, 6838, 2018.

Papale, P., Marzocchi, W., and Garg, D.: Global Volume Distribution for Subaerial Volcanism on Earth, J. Geophys. Res., 126, e2021JB021 763, https://doi.org/https://doi.org/10.1029/2021JB021763, e2021JB021763 2021JB021763, 2021.

Parfitt, E. A.: A discussion of the mechanisms of explosive basaltic eruptions, J. Volcanol. Geoth. Res., 134, 77–107, https://www.sciencedirect.com/science/article/abs/pii/S0377027304000137, 2004.

https://doi.org/10.5194/egusphere-2026-2987
Preprint. Discussion started: 8 July 2026

Parfitt, E. A. and Wilson, L.: The 1983–86 Pu'u 'O'o eruption of Kilauea Volcano, Hawaii: a study of dike geometry and eruption mechanisms for a long-lived eruption, J. Volcanol. Geoth. Res., 59, 179–205, https://www.sciencedirect.com/science/article/abs/pii/0377027394900906, 1994.

Parfitt, E. A., Wilson, L., and Neal, C. A.: Factors influencing the height of Hawaiian lava fountains: implications for the use of fountain height as an indicator of magma gas content, Bulletin of Volcanology, 57, 440–450, https://link.springer.com/article/10.1007/BF00300988, 1995.

Parmigiani, A., Faroughi, S., Huber, C., Bachmann, O., and Su, Y.: Bubble accumulation and its role in the evolution of magma reservoirs in the upper crust, Nature, 532, 492–495, 2016.

Plesset, M. S. and Prosperetti, A.: Bubble dynamics and cavitation, Annu. Rev. Fluid Mech., 9, 145–185, https://doi.org/https://doi.org/10.1146/annurev.fl.09.010177.001045, 1977.

Proussevitch, A. A. and Sahagian, D. L.: Dynamics of coupled diffusive and decompressive bubble growth in magmatic systems, Journal of Geophysical Research: Solid Earth, 101, 17 447–17 455, 1996.

Sanchez, L. and Shcherbakov, R.: Temporal scaling of volcanic eruptions, J. Volcanol. Geoth. Res., 247-248, 115–121, https://doi.org/https://doi.org/10.1016/j.jvolgeores.2012.08.004, 2012.

Scandone, R., Cashman, K. V., and Malone, S. D.: Magma supply, magma ascent and the style of volcanic eruptions, Earth Planet. Sci. Lett., 253, 513–529, https://www.sciencedirect.com/science/article/abs/pii/S0012821X06008181, 2007.

Semeraro, M., Gonnella, G., Lippiello, E., and Sarracino, A.: Diffusion Properties of a Brownian Ratchet with Coulomb Friction, Symmetry, 15, https://doi.org/10.3390/sym15010200, 2023.

Shinohara, H.: Excess degassing from volcanoes and its role on eruptive and intrusive activity, Rev. Geophys., 46, https://agupubs.onlinelibrary.wiley.com/doi/full/10.1029/2007RG000244, 2008.

Smoluchowski, M. v.: Drei vortrage uber diffusion, brownsche molekularbewegung und koagulation von kolloidteilchen, Z. Physik., 17, 585–599, https://eudml.org/doc/215805, 1916.

Sparks, R. S. J.: The dynamics of bubble formation and growth in magmas: A review and analysis, J. Volcanol. Geotherm. Res., 3, 1–37, https://doi.org/10.1016/0377-0273(78)90002-1, 1978.

Sparks, R. S. J. and Young, S.: The eruption of Soufrière Hills Volcano, Montserrat (1995–1999): overview of scientific results, Geological Society of London, 2002.

Tilling, R. I., Heliker, C., and Swanson, D. A.: Eruptions of Hawaiian volcanoes-Past, present, and future, Tech. rep., US Geological Survey, https://pubs.usgs.gov/gip/117/, 2010.

Tran, A., Rudolph, M. L., and Manga, M.: Bubble mobility in mud and magmatic volcanoes, Journal of Volcanology and Geothermal Research, 294, 11–24, 2015.

Turcotte, D. L. and Schubert, G.: Geodynamics, Cambridge Univ. Press, New York, https://www.cambridge.org/highereducation/books/geodynamics/E0E847DA9FE68BDB90C2E457791F0C98#overview, 2012.

Venzke, E.: Global Volcanism Program. Volcanoes of the World, v. 4.11. 0 (08 Jun 2022), Smithsonian Institution, https://volcano.si.edu, 2013.

Vergniolle, S. and Brandeis, G.: Strombolian explosions: 1. A large bubble breaking at the surface of a lava column as a source of sound, J. Geophys. Res., 101, 20 433–20 447, https://agupubs.onlinelibrary.wiley.com/doi/10.1029/96JB01178, 1996.

https://doi.org/10.5194/egusphere-2026-2987
Preprint. Discussion started: 8 July 2026

Vergniolle, S. and Jaupart, C.: Separated two-phase flow and basaltic eruptions, J. Geophys. Res., 91, 12 842–12 860, https://agupubs.onlinelibrary.wiley.com/doi/abs/10.1029/JB091iB12p12842?casa_token=e-zqlgAgOxAAAAAA:qKX-C3XYYZY1gK9KKmrTmtZVhzyBEuk4EAHuISJec8LDifF6m-_umcNUsKIThN741umaeiXhrmbk, 1986.

Walker, G. P. L.: Explosive volcanic eruptions - a new classification scheme, Geologische Rundschau, 62, 431–446, https://link.springer.com/article/10.1007/BF01840108, 1973.

Walker, G. P. L., Self, S., and Wilson, L.: Tarawera 1886, New Zealand - a basaltic plinian fissure eruption, J. Volcanol. Geoth. Res., 21, 61–78, https://www.sciencedirect.com/science/article/abs/pii/0377027384900167, 1984.

Williams, S. N.: Plinian airfall deposits of basaltic composition, Geology, 11, 211–214, https://pubs.geoscienceworld.org/gsa/geology/article-abstract/11/4/211/203463/Plinian-airfall-deposits-of-basaltic-composition?redirectedFrom=fulltext, 1983.

Wilson, L.: Relationships between pressure, volatile content and ejecta velocity in three types of volcanic explosion, J. Volcanol. Geoth. Res., 8, 297–313, https://www.sciencedirect.com/science/article/abs/pii/0377027380901109, 1980.

Wilson, L. and Head III, J. W.: Ascent and eruption of basaltic magma on the Earth and Moon, J. Geophys. Res., 86, 2971–3001, https://agupubs.onlinelibrary.wiley.com/doi/10.1029/JB086iB04p02971, 1981.